Neurocomputing 518 (2023) 321–331

Contents lists available at ScienceDirect

Neurocomputing

journal homepage: www.elsevier.com/locate/neucom

Effects of feedback control in small-world neuronal networks interconnected according to a human connectivity map

Adriane S. Reis [a,*], Eduardo L. Brugnago [a], Ricardo L. Viana [b], Antonio M. Batista [c], Kelly C. Iarosz [d], Iberê L. Caldas [a]

[a] Physics Institute, University of São Paulo, 05508-090 São Paulo, SP, Brazil
[b] Department of Physics, Federal University of Paraná, 81531-980 Curitiba, PR, Brazil
[c] Department of Mathematics and Statistics, State University of Ponta Grossa, 84030-900 Ponta Grossa, PR, Brazil
[d] Department of Engineering, Faculty of Telêmaco Borba, 84266-010 Telêmaco Borba, PR, Brazil

ARTICLE INFO

Article history:
Received 22 April 2022
Revised 11 August 2022
Accepted 2 November 2022
Available online 8 November 2022
Communicated by Zidong Wang

Keywords:
Brain simulation
Neuronal network
Small-world network
Neuronal burst
Synchronization suppression

ABSTRACT

In this work, we consider a phenomenological two-dimensional discrete model coupled in a structure of a clustered network to investigate the suppression of neuronal synchronization in a complex network. We constructed a network according to a weighted human connectivity matrix and an adjacency matrix that carries small-world properties. The coupling between neurons is inserted through a chemical synapse term and a neuronal activation function. The neuronal synchronization is measured by the Kuramoto order parameter. We intend to achieve the suppression of burst phase synchronization, and for that, we use a mathematical tool, based on the technique of deep brain stimulation, which consists of applying an external signal to the network after a certain time, causing the bursts to desynchronize. Our results are efficient when applying the feedback method both in the global network and in the cortical regions. We have seen that for cortical regions, synchronization is more difficult to suppress, however, by slightly increasing the perturbation, we are able to achieve the desired effect. This shows that it is possible to use the control efficiently in isolated cortical areas, therefore, we present a new alternative to conventional methods, avoiding to apply the control to the entire network to obtain the same results.

1. Introduction

Motor disorders that affect humans, such as tremors resulting from Parkinson's disease, involuntary movements during epileptic seizures and essential tremors, are associated, as known in the literature in the field of neurosciences, to synchronized neuronal activity [1–4]. Recent studies investigate suppression methods of neuronal firing synchronization and evidence the success of some techniques already implemented. Complementary, advances in the understanding of this phenomenon, as well as the development of techniques aimed at controlling and suppressing the synchronization of neuronal activity, are demonstrated by studies based on computer simulations of neuronal networks, which are mathematically described by graphs that mimic the connections present in the human brain [5–7].

The human brain is divided into two hemispheres, each of which has an inner core made up of white matter and an outer surface, called the cerebral cortex, which is made up of gray matter [8]. Each hemisphere is conventionally divided into four lobes: frontal, parietal, temporal and occipital, each of which is responsible for our ability to develop certain skills and perform different activities functions. The cerebral cortex, the outermost layer of the brain, is a highly developed structure related to the most familiar functions that are associated with our brain [9].

The unit of the network, the neuron, is essential in carrying out different tasks like cognition, sensory functions, motion, etc. A human being has approximately 86 billion neurons, located mostly in the cerebral neocortex [10]. The organization of neurons in the cortex is distributed in layers so that they connect forming a kind of microcircuit [11–14]. Neurons are responsible for transmitting various electrical signals that process and send information through synapses, established between the dendrites and cell bodies of other neurons. These synapses can be electrical or chemical, being the last one due to the transportation of a neurotransmitter transferring information from a neuron (presynaptic) to the target neuron (postsynaptic) [8]. This exchange of signals occurs as a tangle of connections between dendrites and neural axon terminals,

* Corresponding author.
E-mail address: areis@if.usp.br (A.S. Reis).

https://doi.org/10.1016/j.neucom.2022.11.008
0925-2312/

making it possible to treat the entire structure of the cortex as a network.

The distribution of neurons present in the cortex forms a network whose structure and connection are complex. It is common to consider a neural network built from graph models, among them are small-world [15], random [16] or scale-free networks [17]. The insertion of the topology of a network to study the neuronal dynamics is justified by the fact that the synaptic connections between the several neurons form a network, since the neurons will be able to connect to each other both in relation to their neighboring neurons, and in more distant regions, where each cell will continuously receive a few thousand excitatory or inhibitory stimuli from other neurons [18].

In this work we use a clustered network model to simulate the connection architecture of neurons in the cortex. Each cortical area is represented according to a chosen graph model. We choose to work with a clustered network where the cortical areas are constructed according to a small-world network (SW), according to the Newman-Watts algorithm [19] with 200 interneurons. The connection between these networks is performed by a connection matrix conceived through a map of structural connections of the cortex (human connectome) [20–22], and by an adjacency matrix of the SW network. Previous works were developed using cortical connection maps such as the cat connectome [23–25], macaque [26,27] and *c. elegans* [28,29]. Currently, the scientific literature has many researches involving clustered networks using well-known connectomes, including the human [30–32].

Neuronal activity in some regions of the cortex has a fast and a slow time scale, which are characterized by repetitive spikes and bursts activity. This behavior causes the activity of neurons to alternates between a quiescent state and spike trains [33]. To simulate a neuronal network we need, in addition to a graph model, a mathematical model that describes the dynamical behavior of the neuron. We choose a two-dimensional map in which the combination of its parameters and the recurrence between its variables give the equivalent of a spike or a burst in the neuron, this behavior depends directly on the values adopted for the parameters of the map [34].

To verify the collective behavior of neural firing patterns we coupled the map according to a chemical synapse term, the matrix that addresses the connections in and between areas, a neural activation function and an excitation or inhibition potential. By coupling the map, we are making the neurons present their firing activities synchronized. A relevant point to be considered is the high synchronization between neurons. When neurons are out of synchronization, the resulting electrical signal has a very small oscillation amplitude. Conversely, when neurons are synchronized, the resulting signal from each neuron produces a very relevant oscillation amplitude. Recent works have investigated the synchronization of coupled maps networks, using Rulkov neurons [35–38].

In the literature, there are studies of synchronization in neuronal networks based on time delay methods, that simulate neuronal dynamics through other models and consider the intensity of synaptic coupling between cortical areas, as well as the time delay in the propagation of the signal along the axon [39–42]. Here, we are interested in obtaining low levels of phase synchronization of neuronal activity. In this sense, to control burst synchronization in the clustered network we use a method known as time-delayed feedback, which is a widely used method for stabilizing unstable periodic orbits in chaotic attractors [43]. Such method is based on the application of a feedback perturbation, proportional to the deviation of the current state of the system from its state in a period in the past, so that the control signal disappears when orbit stabilization is reached. This method, introduced by Pyragas [43], uses a control signal obtained from the difference between the current system state and the system state delayed by a period of unstable periodic orbits.

We can extend this concept to control burst synchronization in a neuronal network. To assess synchronization suppression, it is necessary to monitor the variation of the mean-field of the variable that represents the membrane potential on the map. Once this is done, we insert an external signal, which acts as a disturbance, and then after that, we adjust the amplitude of this signal until we reach the desired effect. This procedure considers the inclusion of a time delay due to the need to calculate the mean-field in real time. Applying the time-delayed feedback in our network has an effect similar to deep brain stimulation (DBS), which is based on the application of electrical impulses in target areas of the brain with the aim that this impulse reduces or suppresses the pathological activities associated with brain dysfunctions. The feedback control alied to time-delay has shown successful results to suppress synchronous behaviors and several studies have been done using the technique [44–47].

The structure of this paper is as follows. In Section 2 we present the global network connection model built according to the human connectivity matrix. Section 3 introduces the mathematical model of the neuron and also of the coupled neural network. Section 4 introduces the mechanisms to suppress, or significantly reduce, neuronal synchronization. Finally, in Section 5, we present our conclusions.

2. Corticocortical connection matrix construction

The connections of neural fibers are structured through a connection map, known as a connectome [48]. To build the connection scheme in this paper, we use a human connectivity matrix, assigns links to different cortical areas in an addressed manner [48,49]. Some researches have used different connectomes as a way to simulate synaptic connections in neuronal networks, such as the connectome of *C. elegans* [28], cat [37], macaque [26] and humans [50].

The data used to construct the corticocortical connection matrix were collected and processed by the PIT Bioinformatics group based on data from the NIH-funded Human Connectome Project, and are available at http://braingraph.org [20–22].

According to the original data obtained from the PIT group, we construct a weighted connectivity matrix of healthy human brain, employed for establishing the corticocortical connections, that is, the connection between different cortical areas. The procedure to construct the connectivity matrix is done according steps as follow:

i. Acquiring the average matrix of the amount of neuronal fibers between each pair of cortical areas [51], computed over data from 1064 brains, parceled into 83 nodes resolution, according to the method described in the references [20–22]. This is the upper triangular matrix shown in Fig. 1(a);
ii. Obtaining the histogram with the distribution of the values contained in the matrix resulting from step i, discarding the zeros;
iii. Separate the distribution obtained in step ii into four quartiles and assign the weights:
   0 (1-st quartile, less number of connections);
   1 (2-nd quartile, sparse connectivity);
   2 (3-th quartile, moderate connectivity);
   3 (4-th quartile, dense connectivity).
iv. Formation of the matrix $\mathbb{T}$, shown in Fig. 1(b), by replacing the values in the matrix obtained in step i by the corresponding weights, according to step iii;
v. Getting the connectivity matrix $\mathbb{W} = \mathbb{T} + \mathbb{T}^{\top}$, shown in Fig. 1 (c).

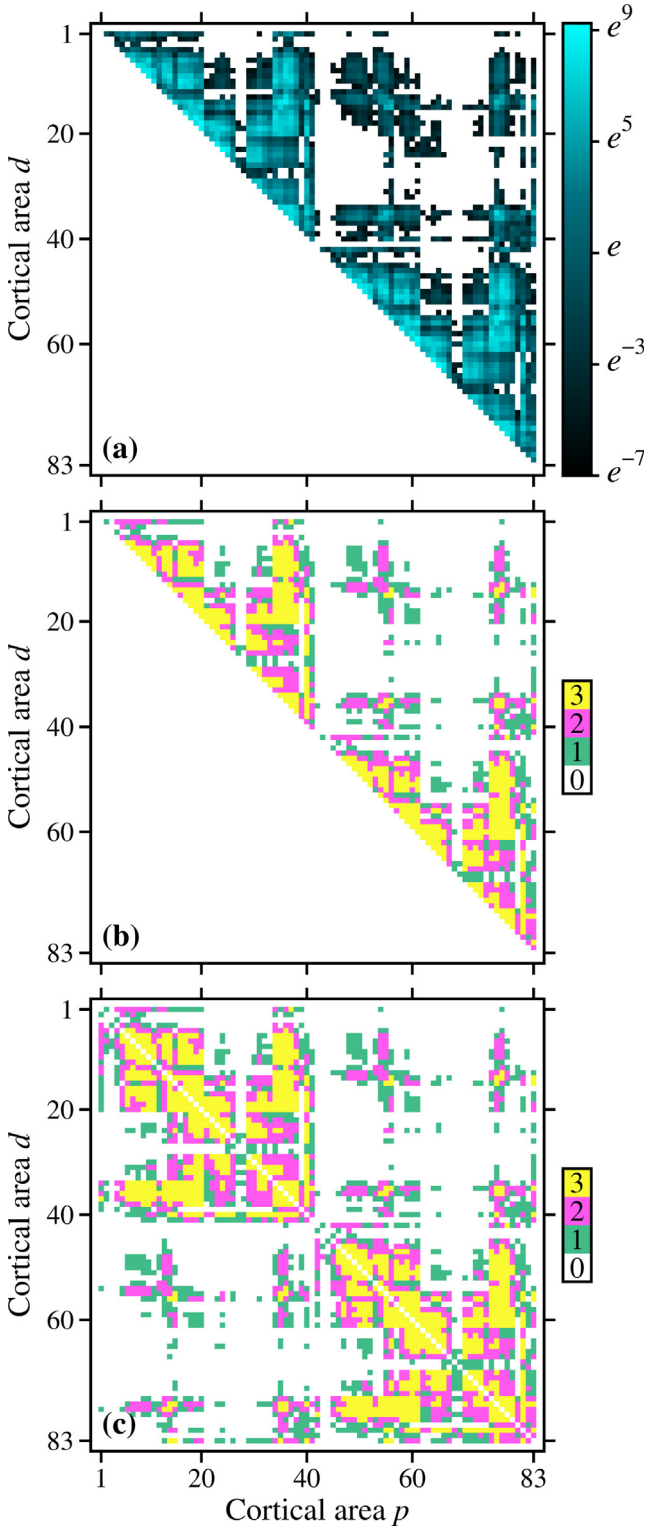

Fig. 1. Sequence of intermediate matrices until obtaining the $\mathbb{W}$ connectivity matrix. Note that the vertical axis is oriented from top to bottom. (a) Average matrix of the amount of neuronal fibers between each pair of cortical areas. The amount of fibers is represented according to the color bar. Blank regions, in the upper triangular, indicate no connections. (b) Upper triangular weight matrix $\mathbb{T}$. Colors indicate the weights of corticocortical connections from 0 (white) to 3 (yellow), according to the label. (c) Complete $\mathbb{W}$ connectivity matrix. Same color code used in the representation of the $\mathbb{T}$ matrix, in detail: 0 – no connections (white), 1 – sparse connections (teal), 2 – moderate connections (magenta) and 3 – dense connections (yellow). (For interpretation of the references to colour in this figure legend, the reader is referred to the web version of this article.)

The weights follow the number of links to be attributed in distinct areas, as determined: 0 – none, 1 – sparse, 2 – moderate and 3 – dense connections. This means that if the weight is 1, 16 connections will be established between two distinct cortical areas. For weights 2, 3 and 0 we add 32, 48 and 0 connections to different cortical areas, respectively. The choice of which pair of cortical areas are connected it is equally drawn.

It is important to make clear that the matrix resulting from the number of fibers gives us an upper triangular matrix, that is, each pair of cortical areas establishes a connection under the condition $p < d$, that is because the data is organized like this in the primary source. Thus, we can make a reflection of the upper triangular matrix $\mathbb{T}$, shown in Fig. 1(b), to obtain the connectivity matrix $\mathbb{W}$, shown in Fig. 1(c). The matrix shown in Fig. 1(c) performs the corticocortical connections in our model, that is, the external connections which are established between different cortical areas.

3. Neuronal dynamics

3.1. Neuronal model

To simulate the neuronal behavior, we use a two-dimensional map given by the following equations:

$$x_{n+1}^{(p,i)} = \frac{\alpha^{(p,i)}}{1 + \left(x_n^{(p,i)}\right)^2} + y_n^{(p,i)}, \tag{1}$$

$$y_{n+1}^{(p,i)} = y_n^{(p,i)} - \sigma\left(x_n^{(p,i)} - \rho\right). \tag{2}$$

This nonlinear system represents the Rulkov map. The typical values for the parameters, that lies in burst regime, are $\rho = -1$, $\sigma = 10^{-3}$ and $\alpha^{(p,i)} \in [4.1, 4.2)$, which are assigned in the computer simulations [34]. Duly adapted to the notation of the network structure, the upper indices p and i correspond to the subnetwork (cortical region) and vertex (neuron) in it, respectively. The lower index n (and $n+1$) marks the evolution in discrete time, corresponds to the iteration state of the map. The diversity in the neuronal population is obtained through distinct $\alpha^{(p,i)}$ randomly determined, with uniform distribution in the refered real half-open interval $[4.1, 4.2)$, for each i-th neuron in the p-th cortical region.

3.2. Network connectivity

The implemented network model is organized into two stages, which are ties-in neurons in the same cortical area, identified as internal connections, and links between different cortical areas, called external connections. All links are chemical type, that is, unidirectional from pre-synaptic to postsynaptic neuron. The subnetworks are built according to the Newmann-Watts algorithm for a small-world network [19], with 200 neurons connected in ring, with 6 nearest neighbors (both left and right sides) and with the probability to add new connections set (shortcuts) as 20%. Thus, there are 1200 inputs from nearby neurons and approximately 40 shortcuts in each simulated cortical area. Furthermore, we guarantee that all neurons have at least one input and one output connection within the same cortical area, as well as no autoconnections occur.

External connections are established according to the connectivity matrix $\mathbb{W}$, represented in Fig. 1(c) and described in Section 2. The number of links between pairs of subnetworks is defined as the correspondent weight in $\mathbb{W}$ multiplied by the factor $\eta = 16$. Given two cortical areas p and d, $\eta W_{p,d}$ pairs of neurons (i, j) are randomly selected, with uniform distribution, being i a vertex of p and j of the d network. The direction of the link is also randomly assigned, with a probability of one half from i to j, or vice versa. In this way, non-

symmetric matrices encoding the simulated corticocortical inputs are obtained. Considering the block matrix $\mathbb{M}_{(83\times83)(200\times200)}$, that encodes just the inputs, the element $M_{(p,d)(i,j)} = W_{p,d}$ is the weighted link from the i-th neuron of the d-th cortical region to the j-th neuron of the d-th region, if there is this chemical connection and being $p \neq d$. However, if this pair of neurons does not have a chemical connection in the described direction, we have $M_{(p,d)(i,j)} = 0$. The submatrices of the diagonal $\mathbb{M}_{(p,p)}$ express the internal connections, whose weights are unitary. Given the type of synaptic connection chosen, the connectivity matrix is not symmetrical, since, in chemical synapses, the neurotransmitter is sent from the presynaptic to the postsynaptic neuron, which makes the process of sending information one way.

Since we aim to simulate a neuronal network where the neurons interact by means of chemical synaptic connections, we couple the neurons by a convenient modification in the Eqs. 1,2. For that purpose, we add a coupling term $-\varepsilon_c C_n^{(p,i)}$ to the first variable, while the second equation of the Rulkov map remains unchanged [30], being

$$x_{n+1}^{(p,i)} = \frac{\alpha^{(p,i)}}{1+\left(x_n^{(p,i)}\right)^2} + y_n^{(p,i)} - \varepsilon_c C_n^{(p,i)}, \tag{3}$$

where the chemical coupling strength $\varepsilon_c \geqslant 0$ and the input coupling factor is defined by

$$C_n^{(p,i)} := \frac{1}{K^{(p,i)}} \sum_{d=1}^{N} \sum_{j=1}^{V} M_{(d,p)(j,i)} \mathscr{H}\left(x_n^{(d,j)} - \theta\right)\left(x_n^{(p,i)} - P_{(d,p)(j,i)}\right). \tag{4}$$

The summation indexes run through the numbers of subnetworks $N = 83$ and vertices $V = 200$ in each one of them. Note that, since there are no autoconnections, we have $M_{(p,p)(i,i)} = 0$. The denominator $K^{(p,i)}$ is the amount of links for the respective neuron, summing the total of inputs from both sources, internal and external connections. As the neuronal activation function, we employ the Heaviside function with the threshold potential $\theta = -1$, set to assume two values:

$$\mathscr{H}\left(x_n^{(d,j)} - \theta\right) = \begin{cases} 0, & \text{if } x_n^{(d,j)} < \theta, \\ 1, & \text{else.} \end{cases} \tag{5}$$

The potential of connection could be excitatory or inhibitory. In our model we choose to set randomly 80% of excitatory and 20% of inhibitory links, respectively. If the synapse is excitatory, the potential takes on the value $P_{(p,d)(i,j)} = 1$, else, $P_{(p,d)(i,j)} = -0.5$.

The input coupling factor can be rewritten in two parts: the first one is relative to internal connections, $p = d$ in Eq. (4), and the adjacency matrix of p-th subnetwork is given by $\mathbb{A}^{(p)} = \mathbb{M}_{(p,p)}$; the second part is relative to external links, $p \neq d$ in Eq. (4). Note that the $\mathbb{A}^{(p)}$ adjacency matrix describes a SW network with unidirectional links, therefore not symmetrical. The element $A_{i,j}^{(p)} = 1$ means that in the p-th cortical area is a chemical connection from the i-th neuron to the j-th one; $A_{i,j}^{(p)} = 0$ means that there is no link with this described orientation. Thus, we obtain the following expression describing separately the intracortical and corticocortical contributions:

$$\begin{aligned} C_n^{(p,i)} := {} & \tfrac{1}{K^{(p,i)}} \sum_{j=1}^{V} A_{j,i}^{(p)} \times \\ & \times \mathscr{H}\left(x_n^{(p,j)} - \theta\right)\left(x_n^{(p,i)} - P_{(p,p)(j,i)}\right) + \\ & + \tfrac{1}{K^{(p,i)}} \sum_{d=1 d\neq p}^{N} \sum_{j=1}^{V} M_{(d,p)(j,i)} \times \\ & \times \mathscr{H}\left(x_n^{(d,j)} - \theta\right)\left(x_n^{(p,i)} - P_{(d,p)(j,i)}\right). \end{aligned} \tag{6}$$

3.3. Phase synchronization

The Rulkov model shows repetitive bursts after periods of quiescent behavior. The onset of each burst in variable $x_{n+1}^{(p,i)}$ of the map is closely related to the variable $y_{n+1}^{(p,i)}$. When a burst starts, the variable $y_{n+1}^{(p,i)}$ has a local maximum, shown in the Fig. 2. In this way, we define a geometric phase in the interval $[0, 2\pi)$ such that

$$\varphi_n^{(p,i)} = 2\pi \frac{n - k_q^{(p,i)}}{k_{q+1}^{(p,i)} - k_q^{(p,i)}}, \tag{7}$$

where $k_q^{(p,i)}$ is the iteration step (discrete time) when q-th burst starts and $k_q^{(p,i)} \leqslant n < k_{q+1}^{(p,i)}$, the phase $\varphi_n^{(p,i)}$ grows monotonically in this time interval. For each neuron, the first burst after the transient receives the index $q = 0$.

The phase synchronization of a set of oscillators can be measured by the Kuramoto order parameter [52], which evaluates the phase state of coupled oscillators classifying their movement

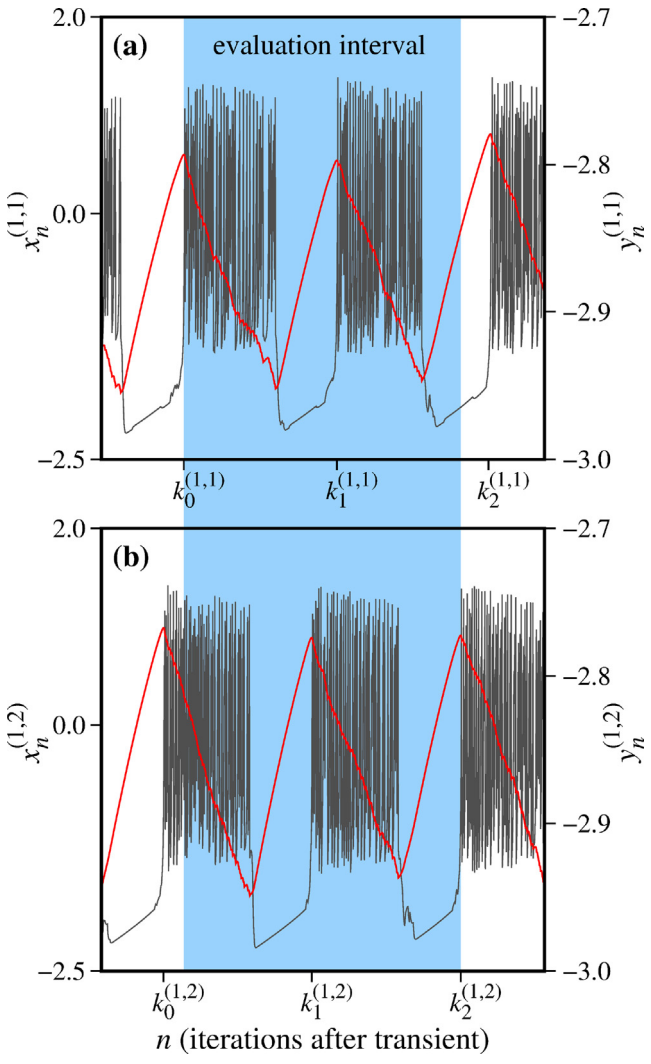

Fig. 2. Time series of coupled map, according to Eq. (3). The Figure show the sequence of bursts in the fast variable $x_n^{(p,i)}$ (gray) and oscillations of the slow variable $y_n^{(p,i)}$ (red line). The burst onset coincides with the local maxima in the $y_n^{(p,i)}$ series, and the starting firing times are exhibited on the horizontal axis. The blue background corresponds to the evaluation interval of the phase synchronization between the two neurons used as an example, both from network 1, namely: (a) first and (b) second neuron. (For interpretation of the references to colour in this figure legend, the reader is referred to the web version of this article.)

as coherent or incoherent. The first one occurs when the oscillators "lock", causing their phases to be synchronized by the their grouped movement, and the second occurs when the oscillators drift along a unitary circle, that is, there is no synchronization phase synchronization [52]. We can make an analogy for the case where neurons are the phase oscillators [53,54], in this way, we can use the definition made in Eq. (7) to measure the phase of neurons firing in burst.

In order to evaluate the synchronization of the neural network within a time interval, we analyze the time average of the Kuramoto order parameter, which is defined for each subnetwork as

$$R^{(p)} = \frac{1}{(n_b - n_a + 1)} \sum_{n=n_a}^{n_b} \frac{1}{V} \left| \sum_{j=1}^{V} e^{i\varphi_n^{(p,j)}} \right|, \tag{8}$$

where i is the imaginary unit. Similarly, for the global network, we have

$$R_g = \frac{1}{(n_b - n_a + 1)} \sum_{n=n_a}^{n_b} \frac{1}{NV} \left| \sum_{p=1}^{N} \sum_{j=1}^{V} e^{i\varphi_n^{(p,j)}} \right|. \tag{9}$$

The Kuramoto order parameter takes on values between $0 \leqslant R^{(p)}, R_g \leqslant 1$, with $R^{(p)}, R_g = 1$ indicating fully phase synchronization, and $R^{(p)}, R_g = 0$ indicating that the neuronal activity are not synchronized in phase.

Due to the definition of the phase, according to Eq. (7), to determine the average parameters in Eqs. (8) and (9) it is necessary that the chosen time interval is between, at least, two bursts of all neurons considered. Thus, the calculation starts from the largest $k_0^{(p,i)}$. The last compute burst time $k_f^{(p,i)}$ of each neuron must be greater than $k_0^{(p,i)} + \Delta$, where $\Delta + 1$ is the number of iterations taken into account. In Fig. 2, we show excerpts from the time series of two neurons in network 1, both with 3 consecutive bursts. Taking this to illustrate how the evaluation time range lies: blue band highlights the synchronization evaluation interval, which starts at $k_0^{(1,1)}$ (tick in Fig. 2)) and ends one iteration before $k_2^{(1,2)}$ (tick in Fig. 2(b)). In this case $\Delta = k_2^{(1,2)} - k_0^{(1,1)} - 1$ and Eq. (8) becomes, for just two neurons, in this example

$$R_{\text{example}} = \frac{1}{(k_2^{(1,2)} - k_0^{(1,1)})} \sum_{n=k_0^{(1,1)}}^{k_2^{(1,2)}-1} \frac{1}{2} \left| \sum_{j=1}^{2} e^{i\varphi_n^{(1,j)}} \right|. \tag{10}$$

In order to obtain the results presented in this study, we computationally evolve the neuronal network discarding the first 10^4 iterations as transient and evaluated the synchronization, according to Eqs. (8) and (9), along also $\Delta + 1 = 10^4$ iterations. Furthermore, the values are averages among 20 initializations (except for raster plots) from randomly assigned equiprobable initial conditions in the intervals $x_0^{(p,i)} \in [-2, 0)$ and $y_0^{(p,i)} \in [-3, -2.5)$. For each set of initial conditions, a different set of values for $\alpha^{(p,i)}$ is also drawn.

An evaluation of the global network phase synchronization reveals an abrupt transition from the non synchronized to the synchronized state, as illustrated by the blue dotted line in Fig. 3(a). Synchronous behavior of neuronal bursts starts at chemical coupling strength $\varepsilon_c \approx 0.016$. With increasing coupling strength, the global phase synchronization changes from $R_g \approx 0$ to $R_g \approx 0.84$, as of $\varepsilon_c \approx 0.02$. Still in Fig. 3(a), it is possible to observe that, in most cases, the subnetworks are more synchronized than the global network. While the largest value of $R^{(p)}$ is very close to unity, the value of R_g does not reach 0.9. This behavior is represented for the 83 subnetworks by the gray curves. Note that some networks remain with synchronization values below 0.8 even for high values of ε_c. It is also important to make an assessment of how the synchronization of neurons occurs within each cortical area. We present in Fig. 3(b) details of the synchronization in each cortical area as a function of the chemical coupling strength. This behavior is similar to global network, but the subnetworks, in general, have higher synchronization levels than R_g. Also in panel (b) we have the presence of some regions in which the synchronization of cortical areas is close to 0.8, which is below the expected given the majority $R^{(p)}$ values. The low synchronization rate in these cases occurs in networks that establish few connections with other networks, this can be better seen in Fig. 1(c). As the human connectivity matrix shows, the cortical areas corresponding to subnetworks 2, 3, 4, 27, 28, 43, 44, 68 and 69 do not establish many connections with other subnetworks. When there is a connection in the cortical areas mentioned, most of these are sparse and few of them have moderate connections. This causes a slower synchronization growth as a function of ε_c of the subnetworks, which can be seen in Fig. 3 both in panel (a), for the networks with $R^{(p)}$ values below

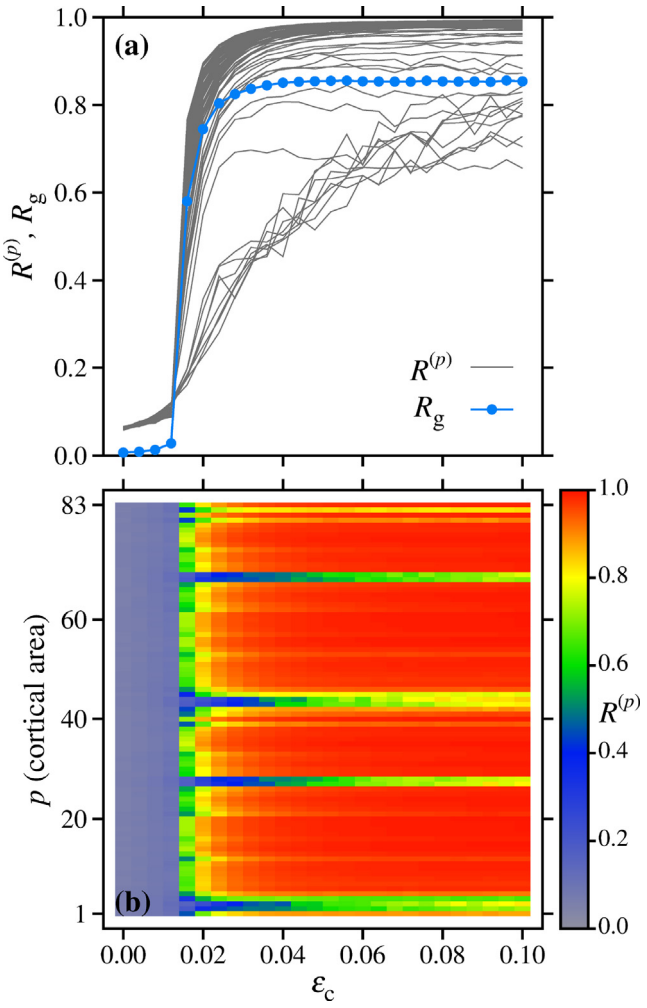

Fig. 3. Phase synchronization as a function of $\varepsilon_c \in [0, 0.1]$ discretized into 26 equidistant values, after discarding the first 10^4 system iterations and calculated the average synchronization along discrete-time of 10^4 steps. For these results, we take on the mean values over the 20 evolutions of the system from randomly assigned initial conditions. In panel (a) are shown the synchronization R_g of the global network (blue dotted line) and $R^{(p)}$ of each subnetwork (gray lines). Panel (b) displays the synchronization details on each subnetwork, $R^{(p)}$ according to palette. (For interpretation of the references to colour in this figure legend, the reader is referred to the web version of this article.)

the average for the global network, and in panel (b), in the regions that go from blue to yellow according the color box.

4. Time-delayed feedback effects

Carry out an assessing synchronization suppression in neuronal dynamics is essential, given the association between high synchronization and neurodegenerative pathologies [1–3]. Thus, finding a method capable of vanishing or decreasing burst synchronization is essential for the neural rhythms to show distinct behavior. The feedback term to be investigated consists of insert a negative term to the equation for the fast variable, proportional to the mean-field $X^{(p)}_{n-\tau}$, considering τ iterations prior to n-th iteration, being the mean-field

$$X^{(p)}_n = \frac{1}{V}\sum_{i=1}^{V} x^{(p,i)}_n. \tag{11}$$

The delayed mean-field for a given cortical region p, is the average of the membrane potential of the network for each neuron in the cortical region considered, remembering that V is the total number of neurons in each subnetwork. In this way, the Eq. (3) receives the feedback term and becomes

$$x^{(p,i)}_{n+1} = \frac{\alpha^{(p,i)}}{1+\left(x^{(p,i)}_n\right)^2} + y^{(p,i)}_n - \varepsilon_c C^{(p,i)}_n - \varepsilon_f \left\lfloor X^{(p)}_{n-\tau} \right\rfloor, \tag{12}$$

where ε_f is the feedback signal strength and τ is the time delay. The floor function applied to the delayed mean-field gives us $\left\lfloor X^{(p)}_{n-\tau} \right\rfloor = z \in \mathbb{Z}$, such that

$$z \leqslant X^{(p)}_{n-\tau} < z+1. \tag{13}$$

This means that z is the largest integer smaller than, or equal to $X^{(p)}_{n-\tau}$ and, according to Eq. (12), a z value is calculated for each subnetwork at every iteration.

The raster plot displayed in Fig. 4 allows us to observe the effect of time-delayed feedback on the neurons of the network. When analyzing the burst synchronization without this term (Fig. 4(a)), we observed the pattern in vertical bands resulting from the phase synchronization of the neuronal bursts, where neurons firing in phase (seen by the red and yellow range) and returning to their quiescent behavior (cyan band), according to the behavior of the map. Once the coupling is added to the map, the neurons lose their phase synchronization, firing at individual rhythms, which is observed by the break in the behavior pattern of the once well-defined bands. For $\varepsilon_f = 0.04$, phase synchronization is not observed, as shown in Fig. 4(b). This evaluation, even if qualitative, is a good indication that synchronization is achieved through the insertion of the coupling term and, with delayed feedback term, this synchronizations is suppressed.

We show, in Fig. 5, the effect of time-delayed feedback control when applied to the neuronal network. In panel (a) we verify through the plot $\tau \times \varepsilon_f$ that there are two distinct regions that exhibit high and low synchronization. The combination of values in the parameter space $\tau \times \varepsilon_f$ for $\varepsilon_f < 0.02$ and all τ values displays a region where network synchronization is still high, reaching $R_g > 0.8$. On the other hand, for τ between 0 and ≈ 16 with combinations of $\varepsilon_f > 0.02$ there is a region of the parameter space where the synchronization presents values of R_g very small, indicating low phase synchronization of neurons in the global network. In panel (b), we have a similar situation. The synchronization suppression occurs for certain combinations of cortical areas and ε_f. In this case, we adopted $\tau = 0$ and see that synchronization in cortical areas decreases as ε_f. Likewise, for values of $\varepsilon_f < 0.02$ there is no supression of synchronization in the neuronal bursts in the sub-

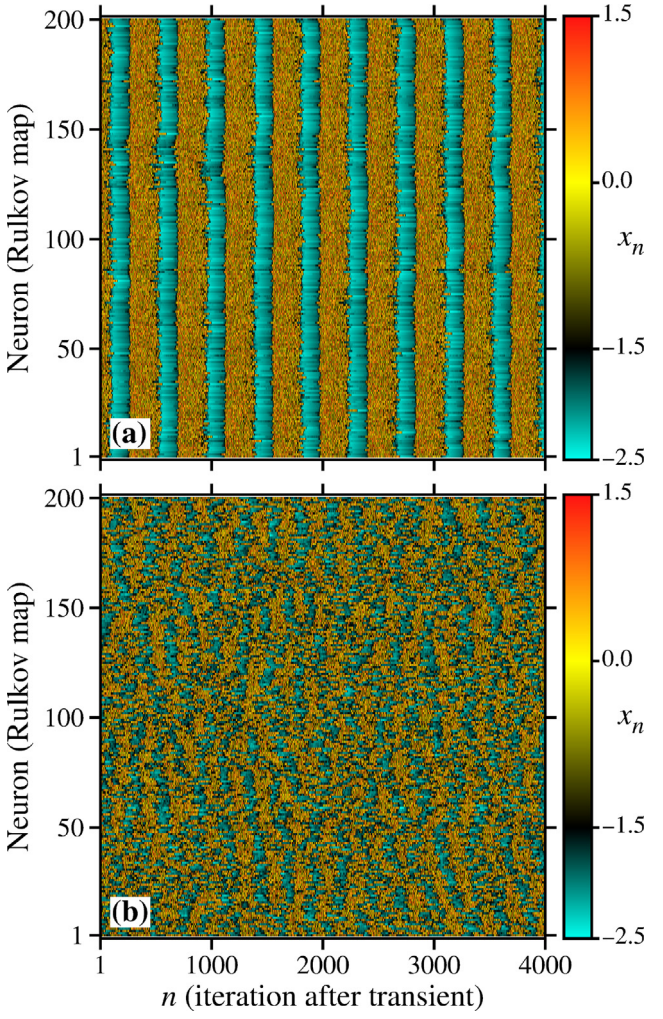

Fig. 4. Raster plot of the fast variables for an example subnetwork. Bursts can be identified in colors from yellow to red and the interval between these is from cyan to black color. In both panels $\varepsilon_c = 0.1$. We observe the evolution of the neural network in two different configurations: (a) Without feedback term, equivalent to $\varepsilon_f = 0$ in Eq. (12). There are well-defined bands over time, evidencing the burst synchronization. (b) With active feedback $\varepsilon_f = 0.04$ and $\tau = 1$. If a well-defined pattern of the bands is not observed, so, there is no synchronization in the phase of neuronal activity. (For interpretation of the references to colour in this figure legend, the reader is referred to the web version of this article.)

networks. So far, we analyze the effectiveness of synchronization suppression through Kuramoto order parameter values, however, the best way to assess the effect of network synchronization control is the suppression measure, which we will introduce in the next subsection.

4.1. Suppresion of global and subnetwork synchronization

The technique used to suppress neuronal burst phase synchronization evaluates the variance according to the mean-field strength [45]. To evaluate the efficiency of the feedback method strategy applied, we compute the synchronization suppression value in each subnetwork, given by

$$S^{(p)} = \sqrt{\frac{\mathrm{Var}\left[X^{(p)}_n(\varepsilon_f = 0)\right]}{\mathrm{Var}\left[X^{(p)}_n\right]}}, \tag{14}$$

being $X^{(p)}_n(\varepsilon_f = 0)$ the mean-field in the absence of the feedback control and $\mathrm{Var}[\cdot]$ denotes the variance. Similarly, we evaluate the global synchronization suppression

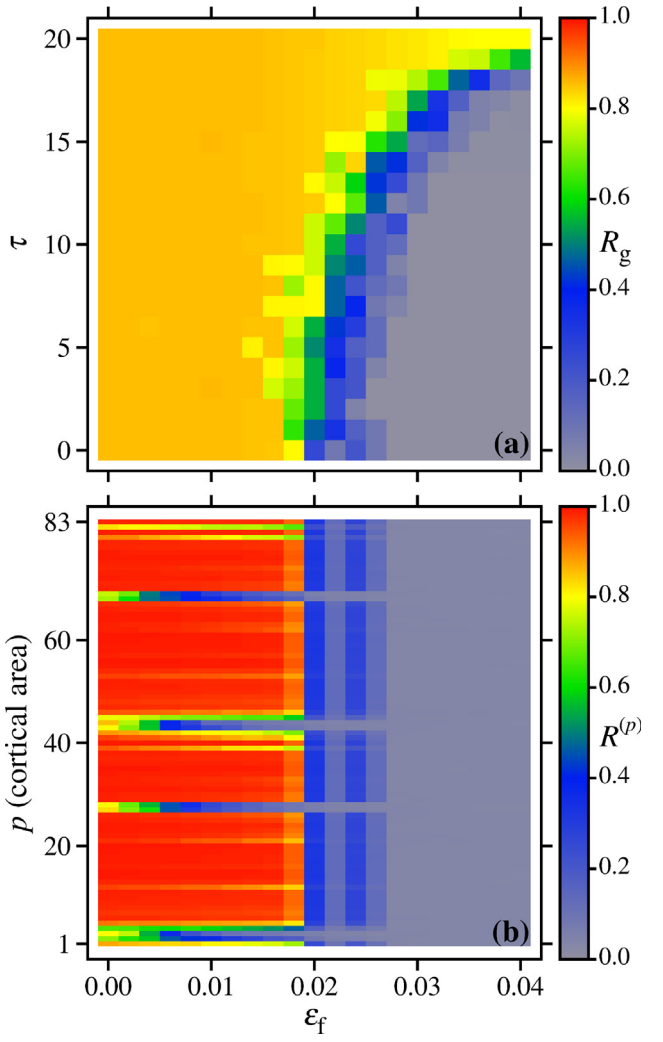

Fig. 5. Network phase synchronization as a function of $\varepsilon_f \in [0, 0.04]$ discretized into 21 equidistant values. We adopted $\varepsilon_c = 0.1$ and the feedback applied throughout the evolution of the system. High synchronized states are represented in color gradient from yellow ($R_g, R^{(p)} = 0.8$) to red ($R_g, R^{(p)} = 1$), lower synchronization is from gray to blue color. (a) Results for global network. Vertical axis are discretized in 21 values for τ from 0 to 20. (b) Evaluation of each subnetwork with delay $\tau = 0$. (For interpretation of the references to colour in this figure legend, the reader is referred to the web version of this article.)

$$S_g = \sqrt{\frac{\mathrm{Var}[\Xi_n(\varepsilon_f = 0)]}{\mathrm{Var}[\Xi_n]}}, \tag{15}$$

where Ξ_n is the mean-field of the fast variable for the global network, given by

$$\Xi_n = \frac{1}{N}\sum_{p=1}^{N} X_n^{(p)} = \frac{1}{NV}\sum_{p=1}^{N}\sum_{i=1}^{V} x_n^{(p,i)}. \tag{16}$$

If an undisturbed subnetwork is phase synchronized at a given interval $n_a \leqslant n < n_b$, the mean-field $X_n^{(p)}(\varepsilon_f = 0)$ presents oscillations accompanying the bursts of neurons [50], being characterized by a well-defined large amplitude oscillations and with a relatively large variance given by $\mathrm{Var}\left[X_n^{(p)}(\varepsilon_f = 0)\right]$. Conversely, if the subnetwork is completely desynchronized, the mean-field exhibits a low amplitude fluctuation, around zero, that is, a low variance [45]. As the objective of the control procedure is to reduce the level of synchronization, we expect that when applying the control term with amplitude ε_f, the variance of the mean-field with control be the smallest possible. Therefore, for the model we are using, the success of the suppression method is reached when the condition $S \gg 1$ is satisfied. The same reasoning is valid for the global network behavior.

Fig. 6 shows the suppression factor obtained for the global network. It is observed, at first, that as we increase the value of the feedback signal strength, the suppression reaches values much greater than the unity, which implies that the chosen method gave us a good Result 6(a). Also, in the panel (a), we see a region, in cyan, that spreads, in which S_g exhibits values lower than 10 for tiny ε_f and certain combinations of ε_c, even when $\varepsilon_c = 0.1$. There is also the presence of a "tongue", region in orange, where the suppression factor reaches the maximum value $S > 100$. The panel (b) shows how synchronization is suppressed in different cortical areas according to the values of ε_f. The plan $p \times \varepsilon_f$ is well separated into two regions whose suppression values are $S^{(p)} < 10$ (dark-cyan) and $S^{(p)} \approx 15$ (yellow), respectively. Within the cortical areas we verify sufficiently high suppression values. Comparing the results of panels (a) and (b), we notice that the suppression in the subnetworks reaches lower values than for the global network, still showing good results for suppressing the neuronal synchronization. We must remember that, as shown in Fig. 3, the synchronization in cortical areas is greater than in the global network, making it more difficult to suppress the synchronization, which corroborates our results.

In order to evaluate the effect of time delay on global synchronization suppression, we compute the value of S_g as a function of τ, with $\varepsilon_c = 0.1$ and for six different values of feedback signal strength. Fig. 7 shows the curves obtained for $0 \leqslant \tau \leqslant 20$, where the adopted values of ε_f are indicated by colors, from $\varepsilon_f = 0.040$ (black line) to $\varepsilon_f = 0.050$ (red line). The suppression value falls with τ, remaining greater than 50 for $\tau \leq 10$ and approximately 25 when $\tau \approx 15$. Such values are still satisfactory as indicative of phase synchronization suppression. However, for $\tau = 20$ none of the feedback signal strengths proved to be sufficient to suppress the synchronization of neuronal activity, with the smaller values $\varepsilon_f = 0.040$ and $\varepsilon_f = 0.042$ (dark-blue line) being insufficient even for the time delay slightly less than 20. Here, we employ feedback signal strength that results in high suppression, the same values are used in the analyzes performed on the Sub-s. 4.2 (see Figs. 8 and 9).

Note that for small values of τ, namely with $\tau = 0$ and $\tau = 1$, we obtain the best global synchronization suppresion levels. In particular, $\tau = 0$ configures the case without delay, being the feedback signal calculated as a function of the cortical area mean-field in the same time of the last iteration. This can be understood by observing that, when a given cortical area presents phase synchronized activity, its mean-field shows oscillations accompanying the neuronal bursts, but the feedback perturbation acts disturbing the current state. Therefore, if most of the neurons are in quiescent state, the feedback acts stimuling firings, if they are in burst, the disturbance is in opposite way. There is suppression of phase synchronization, since different neurons show different responses to stimuli over time.

4.2. Time-delayed feedback acting after synchronization

We also analyze the effect of feedback when applied to an already synchronized network, as the sample shown in Fig. 8. For that, we modify the Eq. 12 by adding a multiplicative time-dependent activation term $\mathscr{H}(\bar{n} - \delta)$, where $\bar{n}$ is the discrete time computed after the transient and δ marks the onset time of feedback actuation. Thus, the networks evolves without the action of a synchronization suppression factor until it is activated from the

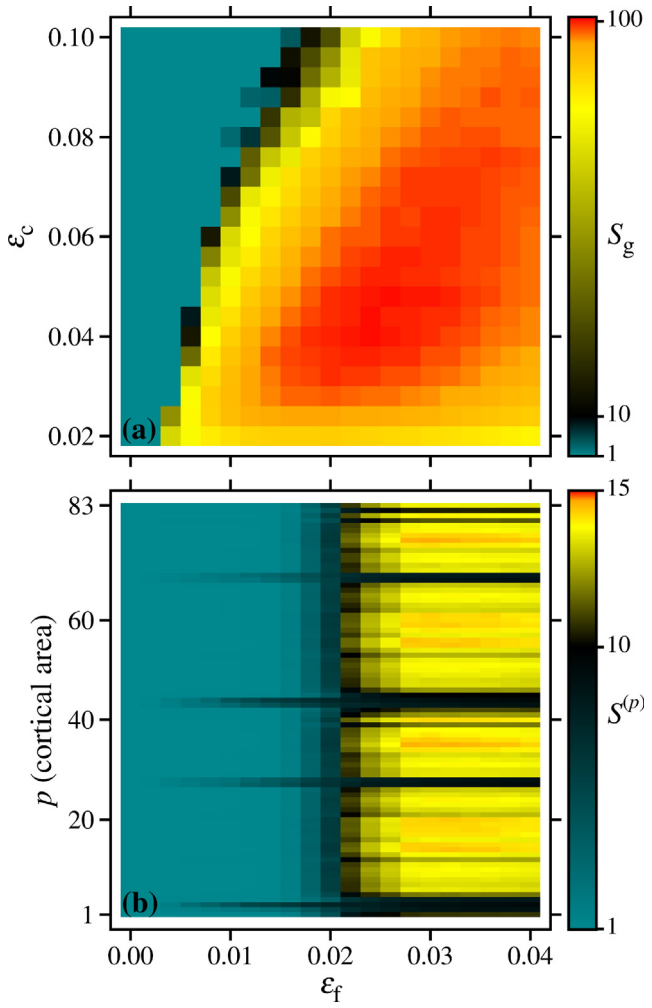

Fig. 6. Synchronization suppression as a function of $\varepsilon_f \in [0, 0.04]$ discretized into 21 equidistant values. Here $\tau = 1$ and the feedback acts throughout the evolution of the system. Suppression values are represented in color, according the palette: lower values in dark-cyan and higher ones in gradient from yellow to red. (a) Global results from pairs $(\varepsilon_f, \varepsilon_c)$, with ε_c varying from 0.02 to 0.1 in steps of 0.004. (b) Detailing for the subnetworks, adopted $\varepsilon_c = 0.1$. (For interpretation of the references to colour in this figure legend, the reader is referred to the web version of this article.)

determined iteration step δ. The fast variable equation takes the form

$$x_{n+1}^{(p,i)} = \frac{\alpha^{(p,i)}}{1+\left(x_n^{(p,i)}\right)^2} + y_n^{(p,i)} - \varepsilon_c C_n^{(p,i)} - \mathscr{H}(\bar{n} - \delta)\varepsilon_f \left| X_{n-\tau}^{(p)} \right|, \tag{17}$$

Here, we define $\delta = 3000$, highlighted in Fig. 8, and evaluate the effect of the feedback signal strengths. This assessment is done by means of temporal evolution of the Kutamoto order parameter, which is calculated for a given subnetwork by

$$r_n^{(p)} = \frac{1}{V}\left| \sum_{j=1}^{V} e^{i\varphi_n^{(p,j)}} \right|. \tag{18}$$

We study the case of high synchronization in the cortical areas. For this, we set $\varepsilon_c = 0.1$ and apply the time started feedback with $\tau = 1$. First, we choose a subnetwork and analyzed how it behaves before and after the feedback control acting in the global network. In Fig. 8, the panel (a) displays the value of $r_n^{(p)}$ according to the temporal evolution from 1000 to 5000 steps after the transient. The panel is divided into two parts that configure without and with the application of feedback, in this order. For the case without feedback, it is expected that the synchronization is high, corroborating the previous results. In this case, the synchronization reaches values of $r_n^{(p)} \approx 1$. From interaction $n = 3000$ after transient, the feedback control acts on the network with $\varepsilon_f = 0.04$ and, as we can see, it does not present a significant reduction in the synchronization value, keeping values close to $r_n^{(p)} = 0.8$. The same effect is observed in the raster plot (panel (b)). Initially, the bursts (yellow) are synchronized in phase followed by their quiescent periods (cyan), and, after the application of the feedback, there is still the presence of well-synchronized firings, characterizing the phase synchronization of Rulkov neurons within the subnetwork.

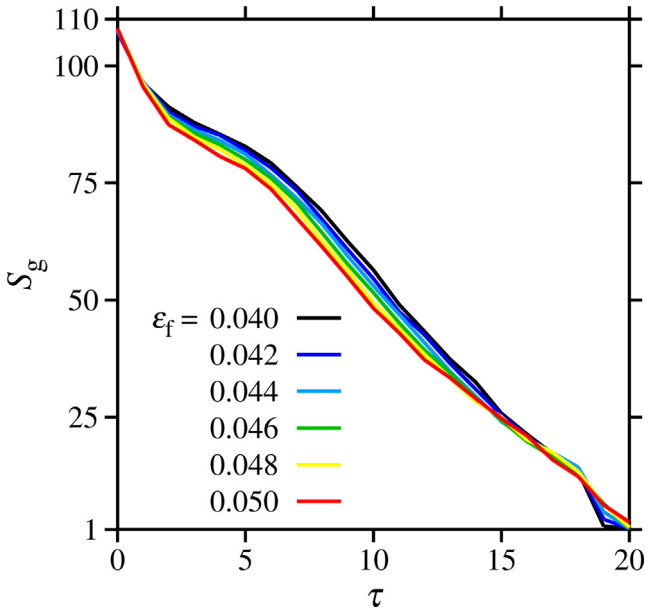

Fig. 7. Suppression of global synchronization as a function of time delay in the interval $0 \leqslant \tau \leqslant 20$. Simulations performed with $\varepsilon_c = 0.1$ for six different ε_f values, according to the label.

We subsequently verified the effect of a stronger feedback signal when applied to the same conditions. Thus, in the panel (c), we see a significant change in the synchronization values before and after the control application. Again, when the feedback is not applied, the phase synchronization has an expected behavior, however, in this case, when applying the control, the synchronization falls quickly, reaching values closely to zero. In the panel (d), the raster plot confirms the control effect. Approximately 500 iterations after starting feedback actuation the phase synchronization falls by half. Around 750 iterations after suppression factor activation, the phase synchronization is completely suppressed, namely the neurons are firing at different times, and it is not possible to distinguish a pattern of yellow bands (bursts) on the raster plot. This evidences that to obtain more expressive results in a given cortical area, it is necessary to apply a slightly larger feedback control signal ε_f, in this case $\varepsilon_f = 0.05$ is enough to achieve the desired effect.

For analyzing the phase synchronization effects of the time started feedback on global network, we perform simulations with six different values of feedback signal strength, being from $\varepsilon_f = 0.040$ to $\varepsilon_f = 0.050$ in steps of 0.002. Similarly to the expression of $r_n^{(p)}$ for an individual network in Eq. (18), the Kuramoto order parameter at a n-th iteration of the global network is given by

$$r_n = \frac{1}{NV}\left| \sum_{p=1}^{N}\sum_{j=1}^{V} e^{i\varphi_n^{(p,j)}} \right|. \tag{19}$$

For simplicity of notation, here we omit the subscript g indicative of global. As in the previous sections, the following results are averages of 20 initialization from randomly initial conditions, which were assigned the same for all ε_f adopted values.

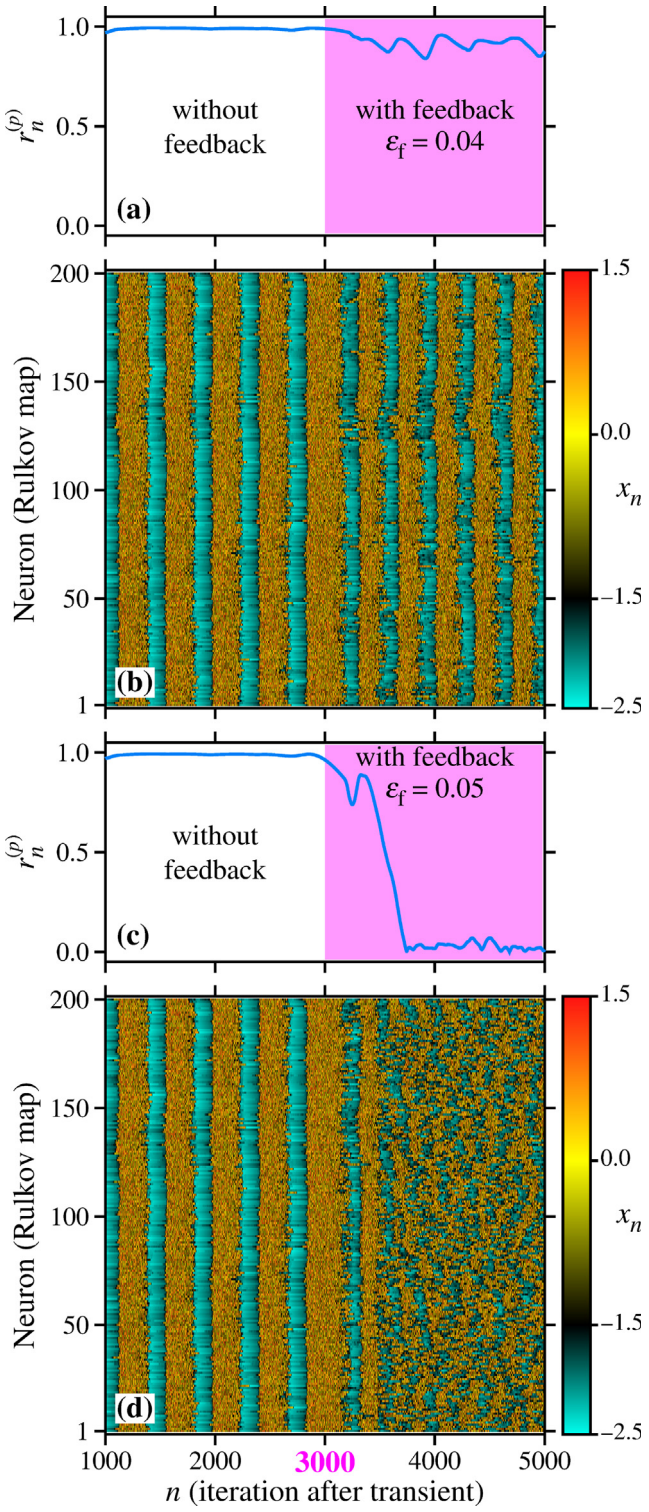

Fig. 8. Effects of applying feedback on the already synchronized global network, shown the behavior of an example cortical region. Chemical coupling strength $\varepsilon_c = 0.1$. Feedback term activated from iteration $n = 3000$ after transient (highlighted on the time axis), delay parameter set as $\tau = 1$. Pink background denotes active feedback term. (a) Evolution of network phase synchronization with $\varepsilon_f = 0.04$. (b) Raster plot of fast variable. The phase synchronization is presented in previous panel. (c) Evolution of network phase synchronization with $\varepsilon_f = 0.05$. (d) Raster plot of fast variable. The phase synchronization is presented in previous panel.

Fig. 9 shows the r_n curves obtained for each feedback signal strength, identified in colors according to the label next to it. Before the activation of the suppression term (white background region),

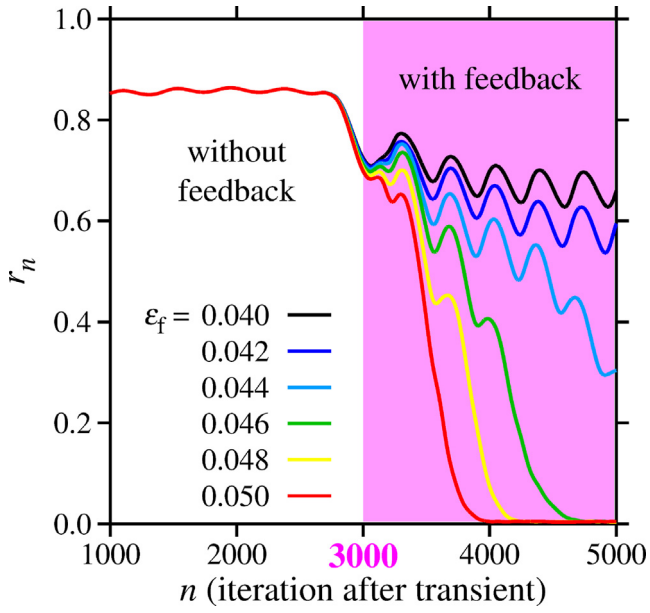

Fig. 9. Effects of applying feedback on the already synchronized global network. The evolution of the Kuramoto order parameter of the global network is shown (Eq. (19)) for six different ε_f values, according to the label, with chemical coupling strength $\varepsilon_c = 0.1$. Feedback term activated from iteration $n = 3000$ after transient (highlighted on the time axis), delay parameter set as $\tau = 1$. Pink background denotes active feedback term.

the global network presents phase synchronization levels oscillating close to $r_n = 0.84$. From the action of the control term (pink background region), in the iteration $n = 3000$ after the transient, different behaviors are observed according to ε_f values. For the highest implemented values $\varepsilon_f = 0.048$ (yellow curve) and $\varepsilon_f = 0.050$ (red curve), a fast reduction in the synchronization of neuronal activity is observed, reaching $r_n \approx 0$ shortly after 1000 iterations with feedback term active with $\varepsilon_f = 0.048$ and, for $\varepsilon_f = 0.050$, a little before this time. A slower decay was obtained with $\varepsilon_f = 0.046$ (green curve), for which complete desynchronization was achieved after 1500 iterations with suppressor term activated. For the three lowest implemented feedback signal strengths, complete desynchronization was not observed in the investigated time interval. $\varepsilon_f = 0.040$ (black curve) and $\varepsilon_f = 0.042$ (dark-blue curve) lead to similar behaviors, with the phase synchronization levels slowly decreasing in oscillations around relatively high values. In these two cases, the suppression method is not satisfactory when applied to the already phase synchronized network. An intermediate behavior is obtained when $\varepsilon_f = 0.044$ (light-blue curve), for which the synchronization of neuronal activity is slowly lost, reaching $r_n \approx 0.3$ at the end of the evaluated time interval.

5. Conclusions

The study of synchronization plays an important role in understanding pathological dysfunctions in certain areas of the cortex. In this work, we employ synchronization control techniques in a small-world network composed of Rulkov neurons, with the network connectivity performed by a human connectivity matrix with 83 cortical areas. Our results indicate that the control method used has a good success rate.

Phase synchronization is evaluated in two situations: (i) in the global network and (ii) in the cortical areas (subnetworks). Comparing the result of the measurement of the Kuramoto order parameter in both cases, we see that for the subnetwork the synchronization is more accentuated, with some networks reaching values higher than in the global network, close to the full phase

synchronization. We understand that this is a characteristic arising from the construction of the network network model, regardless of the chosen network topology, be it small-world, scale-free or random.

The time-delayed feedback technique, applied to all cortical areas in the form of a floor function of the fast variable mean-field in each of them, proved to be quite efficient in suppress the network phase synchronization. When applied to the global network, the success rate is high, with the suppression factor, S_g described in Eq. (15), reaching high values. In contrast, given the high synchronization of neuronal activity, as obtained with chemical coupling strength $\varepsilon_c = 0.1$, the suppression for each cortical area reaches less satisfactory values in some regions. A solution for this is the application of the control with a slight increase of the feedback signal strength (ε_f). The method applied to the network with the neuronal activity already synchronized was effective for $\varepsilon_f \geqslant 0.046$, for which an accentuated desynchronization was observed. On the other side, when applied before phase synchronization, lower values of feedback signal strength, as verified $0.02 < \varepsilon_f \geqslant 0.04$, are sufficient to suppress the synchronization of neuronal activity with the high value of chemical coupling strength $\varepsilon_c \geqslant 0.1$.

The techniques applied in this work allowed us a better understanding of the synchronization of neuronal activity allowing the design of specific recovery strategies based on network analysis. This proved to be important because, in practical terms, it is desirable that external actions in the brain are precisely defined to reach target areas with the application of low currents, which in this study were simulated by the feedback control.

CRediT authorship contribution statement

Adriane S. Reis: Conceptualization, Methodology, Software, Data curation, Writing – original draft, Writing – review & editing, Visualization, Investigation, Validation. **Eduardo L. Brugnago:** Conceptualization, Methodology, Software, Data curation, Writing – original draft, Writing – review & editing, Visualization, Investigation, Validation. **Ricardo L. Viana:** Conceptualization, Methodology, Writing – review & editing, Supervision. **Antonio M. Batista:** Conceptualization, Methodology, Writing - review & editing. **Kelly C. Iarosz:** Methodology, Writing - review & editing. **Iberê L. Caldas:** Conceptualization, Methodology, Writing – review & editing, Supervision.

Declaration of Competing Interest

The authors declare that they have no known competing financial interests or personal relationships that could have appeared to influence the work reported in this paper.

Acknowledgment

This study was possible by the financial support from the following agencies: Brazilian National Council for Scientific and Technological Development (CNPq) under process numbers 161949/2020-7, 407299/2018-1, 302665/2017-0, 301019/2019-3 and 403120/2021-7; Coordination for the Improvement of Higher Education Personnel (CAPES) and São Paulo Research Foundation (FAPESP) under Grant Nos. 2021/12232-0 and 2018/03211-6.

The data that generated the human connectivity matrix were provided (in part) by the Human Connectome Project, WU-Minn Consortium (Principal Investigators: David Van Essen and Kamil Ugurbil; 1U54MH091657) funded by the 16 NIH Institutes and Centers that support the NIH Blueprint for Neuroscience Research; and by the McDonnell Center for Systems Neuroscience at Washington University.

References

[1] C. Hammond, H. Bergman, P. Brown, Pathological synchronization in Parkinson's disease: networks, models and treatments, Trends in Neurosciences 30 (7) (2007) 357–364.
[2] P. Jiruska, M. Curtis, J.G.R. Jefferys, C.A. Schevon, S.J. Schiff, K. Schindler, Synchronization and desynchronization in epilepsy: controversies and hypotheses, Physica D: Nonlinear Phenomena 591 (4) (2013) 787–797.
[3] A. Schnitzler, C. Munks, M. Butz, L. Timmermann, J. Gross, Synchronized brain network associated with essential tremor as revealed by magnetoencephalography, Mov Disord 24 (2009) 1629–1635.
[4] J. Benito-Le'on, J.I. Serrano, E.D. Louis, et al., Essential tremor severity and anatomical changes in brain areas controlling movement sequencing, Ann Clin Transl Neurol 1 (6) (2018) 83–97.
[5] C.A.S. Batista, E.L. Lameu, S.R. Lopes, T. Pereira, G. Zamora-López, R.L. Viana, Phase synchronization of bursting neurons in clustered small-world networks, Phys. Rev. E 86 (2012).
[6] C.A.S. Batista, A.M. Batista, J.A.C. de Pontes, R.L. Viana, S.R. Lopes, Chaotic phase synchronization in scale-free networks of bursting neurons, Phys. Rev. E 76 (1) (2007).
[7] J. Wang, X. Yang, Z. Sun, Suppressing bursting synchronization in a modular neuronal network with synaptic plasticity, Cognitive neurodynamics 12 (6) (2018) 625–636.
[8] M.F. Bear, Connors B.W. Barrt, M.A. Paradiso, Neuroscience: Exploring the Brain, 4th edition,., Wolters Kluwer, Philadelphia, 2016.
[9] Khalid H. Jawabri, Sandeep Sharma, Physiology, Cerebral Cortex Functions. StatPearls Publishing, Treasure Island (FL), 2021.
[10] S. Herculano-Houzel, The human brain in numbers: a linearly scaled-up primate brain, Frontiers in Human Neuroscience 3 (2009) 31.
[11] J.C. Horton, D.L. Adams, The cortical column: a structure without a function, Philosophical transactions of the Royal Society of London 360 (2005) 837–862.
[12] V.B. Mountcastle, The columnar organization of the neocortex, Brain 120 (1997) 701–722.
[13] Gordon. Shepherd, The microcircuit concept applied to cortical evolution: from three-layer to six-layer cortex, Frontiers in Neuroanatomy 5 (2011).
[14] C.R. Noback, D.A. Ruggiero, R.J. Demarest, N.L. Strominger, The Human Nervous System: Structure and Function, 6th edition., Humana Press, Totowa, 2005.
[15] D.J. Watts, S.H. Strogatz, Collective dynamics of 'small-world' networks, Nature 393 (1998) 440.
[16] P. Erdös, A. Rényi, On the evolution of random graphs, Publications of the Mathematical Institute of the Hungarian Academy of Sciences 5 (1960) 17–61.
[17] A.-L. Barabási, R. Albert, Emergence of Scaling in Random Networks, Science 286 (1999) 507–512.
[18] D.R. Chialvo, Generic excitable dynamics on a two-dimensional map, Chaos, Solitons & Fractals 5 (3) (1995) 461–479.
[19] M.E.J. Newman, D.J. Watts, Scaling and percolation in the small-world network model, Physical Review E 60 (6) (1999) 7332–7342.
[20] C. Kerepesi, B. Szalkai, B. Varga, G. Vince, The braingraph.org database of high resolution structural connectomes and the brain graph tools, Cogn Neurodyn 11 (2017) 483–486.
[21] C. Kerepesi, B. Szalkai, B. Varga, G. Vince, How to direct the edges of the connectomes: Dynamics of the consensus connectomes and the development of the connections in the human brain, PLOS ONE 11 (6) (2016) 1–8.
[22] B. Szalkai, C. Kerepesi, B. Varga, G. Vince, High-resolution directed human connectomes and the consensus connectome dynamics, PLOS ONE 14 (4) (2019) 1–11.
[23] J.W. Scannell, G.A.P.C. Burns, C.C. Hilgetag, M.A. O'Neil, M.P. Young, The connectional organization of the cortico-thalamic system of the cat, Cerebral Cortex 9 (3) (1999) 277–299.
[24] J.M. Scannell, M.P. Young, The connectional organization of neural systems in the cat cerebral cortex, Curr. Biol 3 (4) (1993) 191–200.
[25] J.W. Scannell, C. Blakemore, M.P. Young, Analysis of connectivity in the cat cerebral cortex, J. Neurosci 15 (2) (1995) 1463–1483.
[26] Claus-C Hilgetag, Gully APC Burns, Marc A O'Neill, Jack W Scannell, Malcolm P Young, Anatomical connectivity defines the organization of clusters of cortical areas in the macaque and the cat, Philosophical Transactions of the Royal Society of London. Series B: Biological Sciences 355 (1393) (2000) 91–110.
[27] K. Shen, G. Bezgin, M. Schirner, et al., A macaque connectome for large-scale network simulations in thevirtualbrain, Sci Data 6 (123) (2019).
[28] J.G. White, E. Southgate, J.N. Thomson, S. Brenner, The structure of the nervous system of the nematode caenorhabditis elegans, Phil. Trans. 314 (1165) (1986) 1–340.
[29] L.R. Varshney, B.L. Chen, E. Paniagua, D.H. Hall, D.B. Chklovskii, Structural properties of the caenorhabditis elegans neuronal network, PLoS Computational Biology 7 (2) (2011).
[30] F.A.S. Ferrari, R.L. Viana, A.S. Reis, K.C. Iarosz, I.L. Caldas, A.M. Batista, A network of networks model to study phase synchronization using structural connection matrix of human brain, Physica A: Statistical Mechanics and its Applications 496 (2018) 162–170.
[31] A.S. Reis, K.C. Iarosz, F.A.S. Ferrari, I.L. Caldas, A.M. Batista, R.L. Viana, Bursting synchronisation in neuronal assemblies of scale-free networks, Chaos, Solitons & Fractals (2020) 110395.
[32] P.R. Protachevicz, R.R. Borges, A.S. Reis, F.S. Borges, K.C. Iarosz, I.L. Caldas, E.L. Lameu, E.E.N. Macau, R.L. Viana, I.M. Sokolov, F.A.S. Ferrari, J. Kurths, A.M. Batista, C.-Y. Lo, Y. He, C.-P. Lin, Synchronous behaviour in network model

based on human cortico-cortical connections, Physiological Measurement 39 (7) (2018).
[33] Igor Belykh, Enno de Lange, Martin Hasler, Synchronization of bursting neurons: What matters in the network topology, Phys. Rev. Lett. 94 (2005).
[34] N.F. Rulkov, Modelling of spiking-bursting neural behavior using two-dimension map, Phys. Rev. E 65 (2002) 41922.
[35] J.C.A. Pontes, R.L. Viana, S.R. Lopes, C.A.S. Batista, A.M. Batista, Bursting synchronization in non-locally coupled maps, Physica A: Statistical Mechanics and its Applications 387 (16) (2008) 4417–4428.
[36] J.A.S. Paludo, P.R. Protachevicz, R.L. Viana, A.M. Batista, Effects of burst-timing-dependent plasticity on synchronous behaviour in neuronal network, Neurocomputing 436 (2021) 126–135.
[37] E.L. Lameu, F.S. Borges, R.R. Borges, K.C. Iarosz, I.L. Caldas, A.M. Batista, R.L. Viana, J. Kurths, Suppression of phase synchronisation in network based on cat's brain, Chaos 26 (2016).
[38] M. Mugnaine, A.S. Reis, F.S. Borges, R.R. Borges, F.A.S. Ferrari, K.C. Iarosz, I.L. Caldas, E. Lameu, R.L. Viana, J.D. Szezech, J. Kurths, A.M. Batista, Delayed feedback control of phase synchronisation in a neuronal network model, The European Physical Journal Special Topics 227 (10) (2018) 1151–1160.
[39] C.A. Lea-Carnall, M.A. Montemurro, N.J. Trujillo-Barreto, L.M. Parkes, W. el Deredy, Cortical resonance frequencies emerge from network size and connectivity, PLoS Computational Biology 12 (2016).
[40] J. Cabral, H. Luckhoo, M. Woolrich, M. Joensson, H. Mohseni, A. Baker, M.L. Kringelbach, G. Deco, Exploring mechanisms of spontaneous functional connectivity in meg: How delayed network interactions lead to structured amplitude envelopes of band-pass filtered oscillations, NeuroImage 90 (2014) 423–435.
[41] G. Deco, V. Jirsa, A.R. McIntosh, O. Sporns, and R. Kötter. Key role of coupling, delay, and noise in resting brain fluctuations. Proceedings of the National Academy of Sciences, 106(25), 10302–10307, 2009.
[42] A. Ghosh, Y. Rho, A.R. McIntosh, R. Kötter, V. Jirsa, Cortical network dynamics with time delays reveals functional connectivity in the resting brain, Cognitive Neurodynamics 2 (115) (2008) 115–120.
[43] K. Pyragas, Delayed feedback control of chaos, Phil. Trans. R. Soc. A 364 (1846) (2006) 2309–2334.
[44] M.G. Rosenblum, A. Pikovsky, Delayed feedback control of collective synchrony: An approach to suppression of pathological brain rhythms, Phys. Rev. E 70 (2004).
[45] M.G. Rosenblum, A. Pikovsky, Controlling synchronization in an ensemble of globally coupled oscillators, Phys. Rev. Lett. 92 (11) (2004) 102–114.
[46] A. Pikovsky, M. Rosenblum, J. Kurths, Phase synchronization in regular and chaotic systems, International Journal of Bifurcation and Chaos 10 (2000).
[47] C.A.S. Batista, S.R. Lopes, R.L. Viana, A.M. Batista, Delayed feedback control of bursting synchronization in a scale-free network, Neural Networks 23 (2010) 114–124.
[48] O. Sporns, G. Tononi, R. Kötter, The human connectome: A structural description of the human brain, PLOS Computational Biology 1 (4) (2005) 0245–0251.
[49] A.W. Toga, K.A. Clark, P.M. Thompson, D.W. Shattuck, J.D. Van Horn, Mapping the human connectome, Neurosurgery 71 (1) (2012) 1–5.
[50] A.S. Reis, E.L. Brugnago, I.L. Caldas, A.M. Batista, K.C. Iarosz, F. Ferrari, R.L. Viana, Suppression of chaotic bursting synchronization in clustered scale-free networks by an external feedback signal, Chaos 31 (2021).
[51] T.E. Conturo, N.F. Lori, T.S. Cull, E. Akbudak, A.Z. Snyder, J.S. Shimony, R.C. McKinstry, H. Burton, and M.E. Raichle. Tracking neuronal fiber pathways in the living human brain. Proceedings of the National Academy of Sciences of the United States of America, 96(18), 10422–10427, 1999.
[52] Y. Kuramoto, Chemical oscillations, waves, and turbulence, 8th edition., Springer-Verlag, Berlin, 1984.
[53] A. Pikovsky, M.G. Rosenblum, J. Kurths, Phase synchronization of chaotic oscillators, Phys. Rev. Lett. 78 (11) (1996) 1804–1807.
[54] E.L. Lameu, C.A.S. Batista, A.M. Batista, K.C. Iarosz, R.L. Viana, S.R. Lopes, J. Kurths, Suppression of bursting synchronization in clustered scale-free (rich-club) neuronal networks, Chaos 22 (2012).

Adriane da Silva Reis has a degree in Physics (2014), Master's degree in condensed matter physics (2016) and a PhD at Federal University of Paraná in nonlinear dynamics (2021) and postdoctoral fellow at the Physics Institute of University of São Paulo (2021-Currently). She has experience in Physics, working mainly on the following subjects: neuronal networks, suppression of synchronization, nonlinear dynamics, synchronization and complex networks.

Eduardo Luís Brugnago is a postdoctoral fellow at the Physics Institute of USP. PhD in Physics from the Federal University of Paraná (UFPR) in the area of Non-Linear Dynamics. Master and Degree in Physics from the State University of Santa Catarina (UDESC), where he was part of the Non-Linear Dynamics group. He has experience in prediction methods applied to chaotic dynamical systems, analysis based in covariant Lyapunov vectors, computer simulations of dynamical systems and networks, analysis of time series and parameter spaces, coupled maps and chaos suppression.

Ricardo Luiz Viana is a Full Professor in the Physics Department of the Federal University of Paraná, and works there since 1989. He has a D.Sc. in Plasma Physics (São Paulo University, 1991) and completed postdoctoral research in the University of Maryland at College Park (1997) on Nonlinear Dynamics. He is the founder and currently the head of the Plasma Physics and Nonlinear Dynamics Group. His main research subjects are in theoretical plasma physics and applied nonlinear dynamics, including computational neuroscience.

Antonio Marcos Batista is a Bachelor in Physics at the State University of Ponta Grossa (1994), Master of Science at the Federal University of Paraná (1996), PhD in Physics at the Federal University of Paraná (2001), Postdoc in Physics at the University of São Paulo (2004–2006), and Postdoc in Biophysics at Institute for Complex Systems and Mathematical Biology in University of Aberdeen UK (2013–2014). He has experience in Physics, acting on the following subjects: networks, plasma, and biophysics.

Kelly Cristiane Iarosz has a degree in Physics (2015), MSc. in Applied Chemistry (2009) and Ph.D. in Science/Physics at State University of Ponta Grossa (2013). She completed his PhD with a period abroad through the PDSE/CAPES Program at the University of Aberdeen, King's College (Scotland). Postdoctoral in mathematical modeling, physics, complex systems, oscillators and control. She is a reviewer of national and international periodicals, and coordinator of the Exact, Natural and Engineering Sciences area at the Faculty of Telêmaco Borba. She is member of the Postgraduate Programs in Chemical Engineering and Environmental Engineering at the Federal Technological University of Paraná.

Iberê Luiz Caldas has a Bachelor (1970) and PhD. in Physics (1979) from the University of São Paulo (1970). Has experience in Physics, focusing on Physics of Fluids, Plasma Physics, and Electrical Discharges, acting on the following subjects: tokamak, chaos, turbulence, and plasma edge. Since 1995, full professor at the Institute of Physics of the University from São Paulo (Brazil).